

Three-Dimensional Imaging of a Moving Target using an Ultra-Wideband Radar with Five Antennas

Takuya Sakamoto

Graduate School of Informatics
Kyoto University
Kyoto 606-8501, Japan
Email: t-sakamo@i.kyoto-u.ac.jp

Yuji Matsuki

Graduate School of Informatics
Kyoto University
Kyoto 606-8501, Japan

Toru Sato

Graduate School of Informatics
Kyoto University
Kyoto 606-8501, Japan
Email: tsato@kuee.kyoto-u.ac.jp

Abstract—Ultra wideband (UWB) radar systems are a promising technology for surveillance systems. Many of the existing imaging algorithms are based on large-scale antenna arrays that are not necessarily practical because of their complexity and high cost. To resolve this difficulty, we had previously proposed an UWB radar imaging algorithm that estimates unknown 2-dimensional target shapes and motions using only three antennas. In this paper, we extend this method so that 3-dimensional target shapes and motions can be estimated. Some numerical simulations establish that the proposed method can accurately estimate the target shape even under extreme conditions.

Index Terms—ultra-wideband, radar imaging, inverse scattering, 3-dimensional, walking

I. INTRODUCTION

Imaging radars are a promising core technology for next-generation surveillance systems because these can be placed where camera-based systems are not appropriate for use because of resulting privacy issue. It is possible to obtain shapes of human bodies without the associated surface textures by using radars, thus avoiding such concerns. UWB (Ultra Wide-Band) radar is a favored device for this purpose because of its high resolution ranging capability. A variety of imaging algorithms have been proposed for UWB radar systems [1], [2], [3], [4], [5], [6]. However, these conventional imaging methods are based on large-scale antenna arrays, which inevitably make the system too costly to apply in commercial surveillance systems.

To solve this problem and realize a simpler low-cost radar system, we have developed a radar imaging method [7], [8], [9] that exploits the motion of targets, for instance human bodies, rather than a large antenna array setup. Our previous imaging method uses only three antennas, but was still capable of estimating 2-dimensional motion and shapes of targets. However, it is more desirable to obtain 3-dimensional, rather than 2-dimensional, images for actual surveillance applications.

The paper expands the conventional 2-dimensional imaging method to estimate 3-dimensional target motions and shapes. In the conventional 2-dimensional imaging method, a circular model with three parameters was used to approximate a local shape of targets. In our proposed 3-dimensional method, we use a spheroidal model based on five parameters. Therefore, we assume a radar system with five antennas to solve these five

unknowns using received signal data. The performance of the proposed methods is investigated using numerical simulations.

II. SYSTEM MODEL

Figure 1 shows a schematic of the proposed radar system, in which five antennas are installed on a wall of a passage way. The system model is assumed to be 3-dimensional instead of the 2-dimensional system assumed in previous work [7]. The target is modeled as a smooth, convex object with a sharp boundary profile. A reference point on the target surface is chosen to represent the target position $\mathbf{X}_m(t) = (X_m(t), Y_m(t), Z_m(t))$ at time t . The target motion \mathbf{X}_m is assumed to be unknown; only a translational motion without rotation is assumed. The five antennas are in a cruciform arrangement in the $x - z$ plane with separation Δx , i.e. the five antenna coordinates for #1, #2, \dots , #5 are $(\Delta x, 0, 0)$, $(0, 0, 0)$, $(\Delta x, 0, 0)$, $(0, 0, \Delta x)$, $(0, 0, \Delta x)$. Each antenna is assumed omni-directional and connected with a transmitter and receiver with switches, functioning as five independent mono-static radar systems. Transmitted signals are modulated so as not to interfere with the others. The pulse repetition period is set to Δt . The distance between the i -th antenna and the corresponding scattering center at time t is defined as $R_i(t)$ for $i = 1, 2, \dots, 5$. Our purpose in the paper is to estimate the target motion $\mathbf{X}_m(t)$ and shape using these five range data.

III. CONVENTIONAL TWO-DIMENSIONAL IMAGING METHOD

Our previous work [7] proposed a 2-dimensional imaging method. The method uses three antennas #1, #2, and #3 to estimate the shape of a target in non-rotating translational motion. The motion is assumed to be 2-dimensional as well, which means $Z_m(t) = \text{const.}$ in the above-defined motion. The method approximates the local shape of a target with circles termed a curvature circle. A curvature circle has three parameters, a curvature center $\mathbf{c}(t) = (c_x(t), c_y(t))$ and a curvature radius $a(t)$. These parameters are determined by solving the following set of equations.

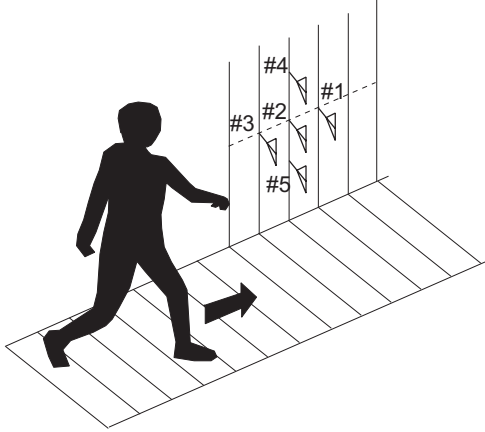


Fig. 1. Proposed radar system for surveillance systems.

$$\begin{cases} R_1(t) = \sqrt{(c_x(t) + \Delta x)^2 + (c_y(t))^2} - a(t) \\ R_2(t) = \sqrt{(c_x(t))^2 + (c_y(t))^2} - a(t) \\ R_3(t) = \sqrt{(c_x(t) - \Delta x)^2 + (c_y(t))^2} - a(t) \end{cases} \quad (1)$$

Note that the motion $\mathbf{c}(t)$ contains not only the target motion $\mathbf{X}(t)$ but also the relative motion of a scattering center along the target surface. Therefore, $(c_x(t), c_y(t))$ cannot be used directly as an estimate of the target motion.

To overcome this difficulty, the proposed method calculates an average radius of curvature with $a(t_n)$ and $a(t_{n+1})$ as $\bar{a}(t_{n+\frac{1}{2}}) = (a(t_n) + a(t_{n+1}))/2$. Then, $\mathbf{c}(t_n)$ and $\mathbf{c}(t_{n+1})$ are recalculated as $\bar{\mathbf{c}}(t_n)$ and $\bar{\mathbf{c}}(t_{n+1})$, subject to the condition that the radius of curvature is equal to $\bar{a}(t_{n+\frac{1}{2}})$ with LMS (Least Mean Square) criteria. An instantaneous velocity vector $\mathbf{v}_{n+\frac{1}{2}}$ is defined as

$$\mathbf{v}_{n+\frac{1}{2}} = (\bar{\mathbf{c}}(t_{n+1}) - \bar{\mathbf{c}}(t_n)) / \Delta t. \quad (2)$$

This operation enables the separation of the target motion $\mathbf{X}(t)$ from the relative motion of the scattering center because the motion of scattering center strongly affects the radius of curvature $a(t)$. In addition, this radius of curvature $a(t)$ together with the target motion $\mathbf{X}(t)$ have a great effect on the center of curvature $\mathbf{c}(t)$. Figure 2 shows a schematic of this procedure, where three circles of curvature for successive time shots $t = t_n, t_{n+1}, t_{n+2}$ have been drawn with dashed lines. The averaged circles of curvature using successive pairs $t = t_n, t_{n+1}$ and t_{n+1}, t_{n+2} are depicted with solid lines. Each velocity vector associated with an average circle is drawn as the arrow from that circle's center to its successive center.

Finally, we integrate the instantaneous velocity vector using the summation form as

$$\bar{\mathbf{X}}(t_{N+\frac{1}{2}}) = \sum_{n=1}^N \mathbf{v}_{n+\frac{1}{2}} \quad (3)$$

to obtain an estimate of the target location $\bar{\mathbf{X}}(t)$. Note that the initial value $\mathbf{X}(0)$ does not have any effect on imaging results

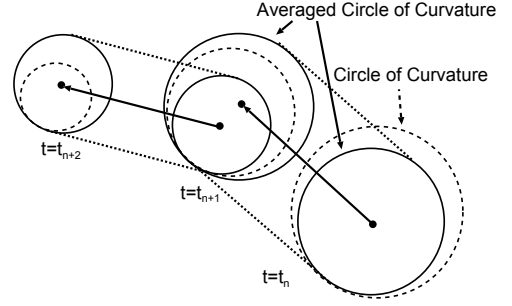


Fig. 2. A schematic of the averaging circles of curvature in the proposed method.

because it affects only the location of the estimated image. By compensating for this estimated target motion $\bar{\mathbf{X}}(t)$, the estimated scattering centers are shifted to the right at $t = 0$ to form a 2-dimensional image.

IV. PROPOSED THREE-DIMENSIONAL IMAGING ALGORITHM

We present an extended version of the above method applicable to three-dimensional cases. This method approximates the local shape of the target with a spheroid instead of a circle. A spheroid is a surface that is obtained by rotating an ellipse about its principal axis. We use all five antennas to estimate the five parameters of a spheroid expressed using a center $\mathbf{c}(t) = (c_x(t), c_y(t), c_z(t))$, and the respective horizontal and vertical radii $a(t)$ and $b(t)$ as

$$\frac{(x - c_x(t))^2}{a(t)^2} + \frac{(y - c_y(t))^2}{a(t)^2} + \frac{(z - c_z(t))^2}{b(t)^2} = 1. \quad (4)$$

Using the five ranging data $Ri(t)$ ($i = 1, 2, \dots, 5$) from the five antennas, these five spheroid parameters are determined with Brent's method [10]. Although translational motion $\mathbf{X}(t)$ can be estimated approximately using these parameters, it is not identical to the center position $\mathbf{c}(t)$ for the same reason as in the two-dimensional case.

The proposed method calculates averaged horizontal and vertical radii using a couple of adjacent samples as $\bar{a}_{n+\frac{1}{2}} = (a(t_n) + a(t_{n+1}))/2$ and $\bar{b}_{n+\frac{1}{2}} = (b(t_n) + b(t_{n+1}))/2$. These averaged radii are then used for recalculating the center positions $\bar{\mathbf{c}}(t_n)$ and $\bar{\mathbf{c}}(t_{n+1})$ with estimated scattering center positions $\mathbf{p}_i(t) = (p_{xi}(t), p_{yi}(t), p_{zi}(t))$ ($i = 1, 2, \dots, 5$). The center positions $\bar{\mathbf{c}}(t_n)$ and $\bar{\mathbf{c}}(t_{n+1})$ are optimized with other parameters fixed as $a = \bar{a}_{n+\frac{1}{2}}$ and $b = \bar{b}_{n+\frac{1}{2}}$ to minimize the distance between the spheroid surface and the scattering centers $\mathbf{p}_i(t_n)$ and $\mathbf{p}_i(t_{n+1})$ ($i = 1, 2, \dots, 5$). Finally, these center positions $\bar{\mathbf{c}}(t_n)$ and $\bar{\mathbf{c}}(t_{n+1})$ are used to calculate an instantaneous velocity vector $\mathbf{v}_{n+\frac{1}{2}} = (\bar{\mathbf{c}}(t_{n+1}) - \bar{\mathbf{c}}(t_n)) / \Delta t$.

Figure 3 shows the difference between the methods with/without the averaging process applied to the horizontal and vertical radii. The averaging of radii was introduced in our proposed method because it can accurately estimate the target translational motion by eliminating the motion of the scattering center on a target surface. This averaging process displaces the

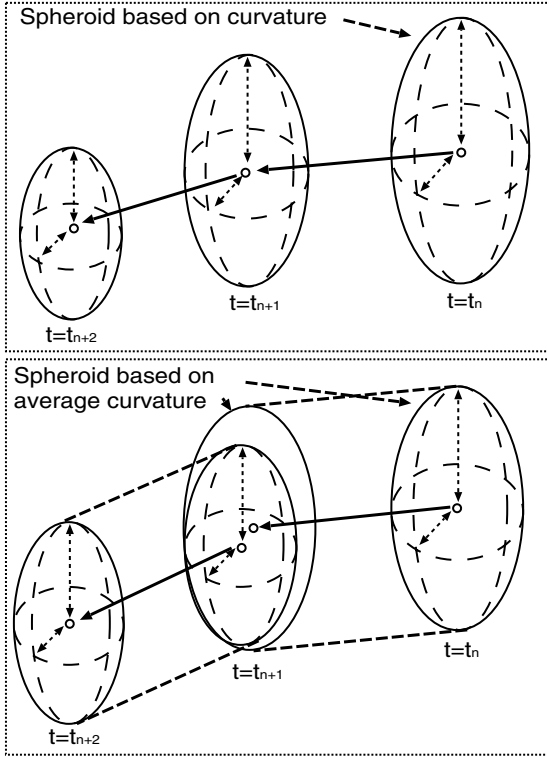


Fig. 3. Estimated velocity vectors using the motion estimation methods with/without the radii averaging.

velocity vectors as shown for the spheroid at $t = t_{n+1}$ in the lower image in Fig. 3. Next, these estimated velocity vectors are summed to obtain the target motion. Finally, the final image is obtained by shifting the scattering center positions $\mathbf{p}_i(t) (i = 1, 2, \dots, 5)$, compensating for the estimated target motion.

After obtaining the image, we apply an artifact suppression method. This method eliminates the point \mathbf{x}_i that satisfies

$$\min_j |\mathbf{x}_i - \mathbf{x}_j| > \Delta d \quad (i \neq j). \quad (5)$$

This method is based on the assumption that most of the artifacts are isolated from other points. Thus, a point separated from other points with minimum Δd -proximity can be eliminated. The value Δd is empirically determined.

V. PERFORMANCE EVALUATION OF THE PROPOSED METHOD

We apply the proposed method to an ellipsoidal target to verify its effectiveness. Figure 4 depicts the assumed ellipsoidal target in translational motion; the ellipsoid has a vertical aspect with x -axis radius $A = 0.15$ m, y -axis radius $B = 0.25$ m, and z -axis radius $C = 0.85$ m. These parameters have been chosen in view of applications to human body imaging. The target motion is $(X_m(t), Y_m(t), Z_m(t)) = (x_0 + v_x t, y_0, z_0 \sin(\omega t + \chi_0))$, where $x_0 = 2.0$ m, $v_x = -1.0$ m/sec, $y_0 = 1.0$ m, $z_0 = 0.25$ m, $\omega = \pi/4$ rad/sec, $\chi_0 = \pi/2$ rad. The antenna separation interval is $\Delta x = 0.5$ m. First, we develop an imaging result under noiseless environments

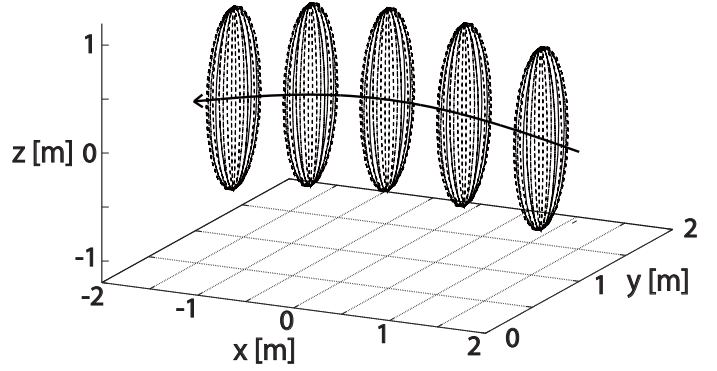


Fig. 4. Assumed target shape and motion for performance evaluation.

using the data sampling interval of $\Delta t = 4$ msec over a sampling period $-2 \text{ sec} \leq t \leq 2 \text{ sec}$. The parameter for artifact suppression is set at $\Delta d = 5.0$ mm; throughout this paper, Δd is fixed at this value.

The proposed method optimizes the spheroidal target using the received data $R_i(t) (i = 1, 2, \dots, 5)$, snapshots of which are shown in Fig. 5. In the figure, the solid and broken lines are the respective actual and estimated target shapes for each time step. These shapes are not identical because our model is spheroidal, not ellipsoidal, which means that our method estimates only a local shape of the target rather than the entire shape. The white dots denote the scattering centers calculated using the received data.

The solid line in Fig. 6 shows the actual target motion. The dashed lines 1 and 2 in Fig. 6 show the central position of the spheroidal model estimated without/with the proposed radii averaging process. The RMS error values of the target motion without/with the proposed radii averaging process are 162.8 mm and 21.5 mm, respectively. This shows the averaging process improves the motion estimation accuracy.

Finally, we estimate the target shape by compensating for the estimated motion using the estimated scattering center points. Figure 7 shows the estimated target shape, where the RMS error of the image is 8.2 mm. In this figure, we see five lines that correspond to the five scattering centers estimated in our method. Since the target moves horizontally, the image has only horizontal profiles as well. This result establishes that our proposed method is capable of estimating an unknown 3-dimensional target motion and ellipsoidal shape accurately.

VI. PERFORMANCE OF THE PROPOSED METHOD UNDER VARIOUS CONDITIONS

A. Imaging Accuracy and Target Shape

We now calculate the imaging accuracy of the proposed method for various values of x -axis-radius A from 0.15 m to 0.5 m. This parameter range is selected based on the statistical range of actual human body shapes. Other parameters remain fixed with those values set in the previous section. Figure 8 shows A -radial dependence of the RMS errors of the various images estimated using the proposed method. The RMS error has a minimum value at $A = 0.25$ m corresponding to an

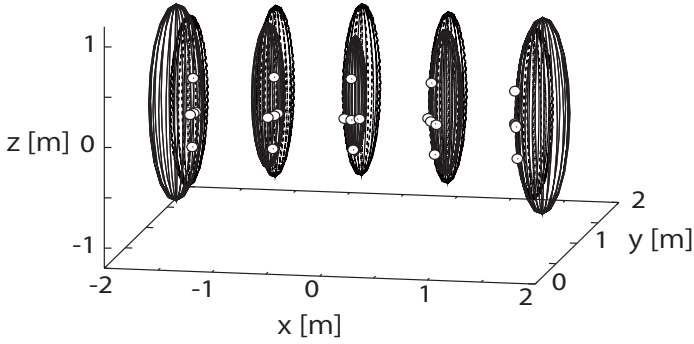


Fig. 5. Actual and estimated target shape using the proposed method.

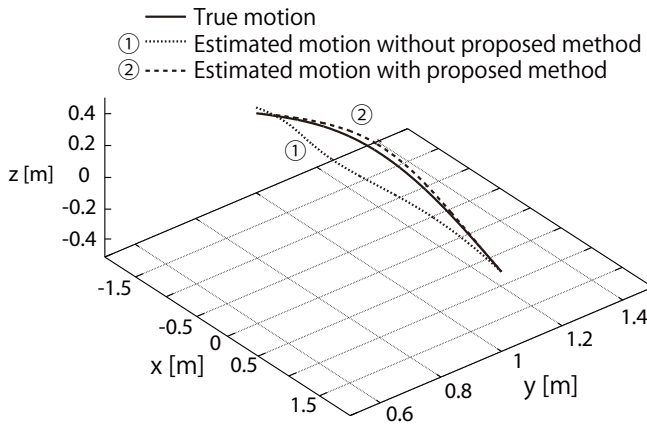


Fig. 6. Estimated translational motion of a target.

ellipsoid target with $A = B$. Since the proposed method assumes a spheroidal model, this specific case corresponds to the ideal case where the model is identical to the actual target shape. For target shapes with $A \neq B$, the RMS error is larger but is less than 11.5 mm over the selected parameter range. This is accurate enough for most applications presumed in the paper.

B. Imaging Accuracy and Target Motion

Next, we investigate the imaging accuracy of the proposed method for various target motions. We assume a target shape as an ellipsoid with $A = 0.15$ m, $B = 0.25$ m and $C = 0.85$ m. The target motion is $(X_m(t), Y_m(t), Z_m(t)) = (x_0 + v_x t, y_0, z_0 \sin(\omega t + \chi_0))$, where $x_0 = 2.0$ m, $v_x = -1.0$ m/sec, $y_0 = 1.0$ m, $\omega = \pi/2$ rad/sec, $\chi_0 = 0$ rad are assumed. We vary the parameter z_0 from 0 m to 0.5 m, which corresponds to a vertical springing motion in normal human gaits.

Figure 9 shows the relationship between the RMS error of the proposed method and the vertical amplitude z_0 . The RMS error values for $z_0 = 0$ m and $z_0 = 0.5$ m are 5.4 mm and 9.2 mm, respectively. The accuracy is degraded as the vertical motion becomes larger.

C. Imaging Accuracy and Antenna Intervals

We investigate the imaging accuracy of the proposed method for various antenna intervals. The target shape is assumed to

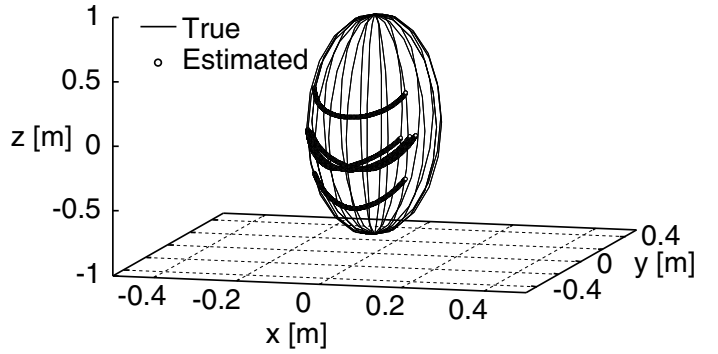


Fig. 7. Estimated target image using proposed method.

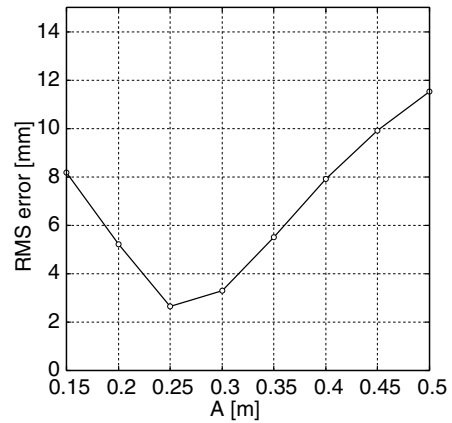


Fig. 8. Relationship between imaging accuracy and target's x -axis radius.

be the same as in the previous section. The target motion is assumed as $(X_m(t), Y_m(t), Z_m(t)) = (x_0 + v_x t, y_0, z_0)$, where $x_0 = 2.0$ m, $v_x = -1.0$ m/sec, $y_0 = 1.0$ m, and $z_0 = 1.0$ m. This modeled motion is uniform along a straight line parallel to the antenna baseline. Here we assume a noiseless environment. Figure 10 shows the RMS error of the motion analyzed by the proposed method for various antenna intervals $0.1 \text{ m} \leq \Delta x \leq 1.0$ m

Clearly, as the antenna interval increases, the imaging error becomes larger mainly for the following reason. For a large antenna interval, the scattering center points are well separated from one another. Because the proposed method approximates the local shape of a target by model fitting, the separated scattering centers do not represent a local shape, making it difficult to apply this approach. As a result, imaging accuracy deteriorates for large Δx .

Note also that within a noisy environment, a small antenna interval increases imaging error sensitivity to background noise. Therefore, an optimum antenna interval should be determined based on the actual signal-to-noise (S/N) ratio of the data.

D. Performance Evaluation in Noisy Environment

Finally, we investigate the imaging accuracy of the proposed method in noisy environments. The assumed target shape and motion will be assumed the same as in the previous section.

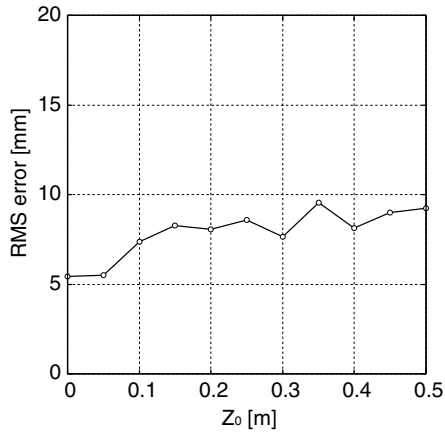


Fig. 9. Relationship between imaging accuracy and vertical target motion parameter z_0 .

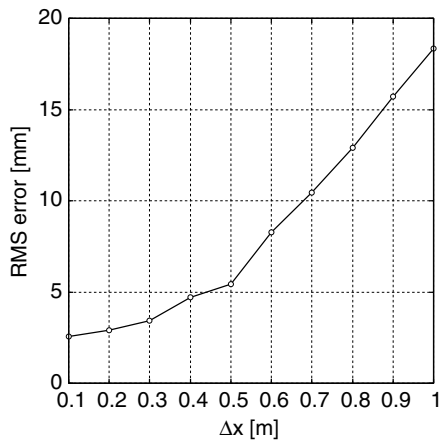


Fig. 10. Relationship between imaging accuracy and antenna interval Δx .

We set the antenna interval $\Delta x = 0.5$ m. White Gaussian random components are added to each of the range data $R_i(t)$ ($i = 1, 2, \dots, 5$) to simulate a noisy environment. The relationship between the squared errors in the range data and the received signal power is linear for large S/N as in [11]. The S/N is defined as the signal and noise power after applying the matched filter. The signal power is calculated based on a free space model, in which the target cross-section dependency is not taken into account. We assume the lowest S/N to be 15 dB, for which the range data $R_i(t)$ has its maximum value. Figure 11 shows the estimated image under these conditions. The RMS error of the image is 6.7 mm, which demonstrates that the proposed method is capable of estimating target shape and motion even in noisy environments. Further study is needed to clarify the necessary system's requirements and minimum S/N for which the proposed method can be applied.

VII. CONCLUSION

In this study, we proposed an imaging method for simple UWB radar systems with five antennas by using the motion of a target. This method estimates a 3-dimensional target motion, and then obtains 3-dimensional target images by compensating

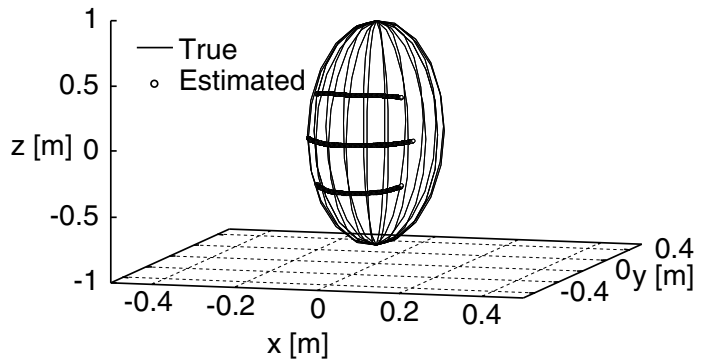


Fig. 11. Estimated target image in a noisy environment with the lowest S/N = 15 dB.

for the motion. This approach is an extension of the conventional 2-dimensional imaging method for three-antenna radar system. The proposed method assumes a spheroidal model to approximate the local shape of a target. The performance of the proposed method has been verified using numerical simulations. The imaging accuracy was also quantitatively evaluated for various models. The simulation results showed that the proposed method can estimate 3-dimensional target shapes in a number of scenarios.

REFERENCES

- [1] C. J. Leuschen and R. G. Plumb, "A matched-filter-based reverse-time migration algorithm for ground-penetrating radar data," *IEEE Trans. Geoscience & Remote Sensing*, vol. 39, no. 5, pp. 929–936, May 2001.
- [2] A. G. Yarovoy, T. G. Savelyev, P. J. Aubry, P. E. Lys, and L. P. Ligthart, "UWB array-based sensor for near-field imaging," *IEEE Transactions on Microwave Theory and Techniques*, vol. 55, no. 6, part 2, pp. 1288–1295, June 2007.
- [3] S. Masuyama and A. Hirose, "Walled LTSA array for rapid, high spatial resolution, and phase-sensitive imaging to visualize plastic landmines," *IEEE Trans. Geoscience and Remote Sensing*, vol. 45, no. 8, pp. 2536–2543, Aug. 2007.
- [4] M. Dehmollaian and K. Sarabandi, "Refocusing through building walls using synthetic aperture radar," *IEEE Trans. Geoscience and Remote Sensing*, vol. 46, no. 6, pp. 1589–1599, June 2008.
- [5] Y. Yang and A. E. Fathy, "Development and implementation of a real-time see-through-wall radar system based on FPGA," *IEEE Trans. Geoscience and Remote Sensing*, vol. 47, no. 5, pp. 1270–1280, May 2009.
- [6] X. Zhuge, A. G. Yarovoy, T. Savelyev, and L. Ligthart, "Modified Kirchhoff migration for UWB MIMO array-based radar imaging," *IEEE Trans. Geoscience and Remote Sensing*, vol. 48, no. 6, pp. 2692–2703, June 2010.
- [7] T. Sakamoto, Y. Matsuki, and T. Sato, "A Novel UWB Radar 2-D Imaging Method with a Small Number of Antennas for Targets with Arbitrary Shapes and Motion," *Proc. 2009 IEEE International Conference on Ultra-WideBand (ICUWB2009)*, pp.449–453, Sep., 2009.
- [8] Y. Matsuki, T. Sakamoto, and T. Sato, "Study of a Method for 2-D Imaging of Simple-Shaped Targets with Arbitrary Motion using UWB Radar with a Small Number of Antennas," *Proc. 20th International Conference on Applied Electromagnetics and Communications (ICECom 2010)*, Sep. 2010.
- [9] Y. Matsuki, T. Sakamoto, and T. Sato, "An Imaging Algorithm of a Target with Arbitrary Motion for Ultra Wide-Band Radar with a Small Number of Antennas," *IEICE Trans. Communications*, Vol.E94-B, No.03, pp.742–749, Mar. 2011.
- [10] R. P. Brent, "Algorithms for Minimization without Derivatives," Prentice Hall, 1972.
- [11] T. Sakamoto, "A 2-D image stabilization algorithm for UWB pulse radars with fractional boundary scattering transform," *IEICE Trans. on Commun.*, vol. E90–B, no. 1, pp. 131–139, Jan. 2007.